

Multi-angle, multi-scale inversion of migrated seismic data: an overview

Kees Wapenaar, Delft Univ. of Techn. Aart-Jan van Wijngaarden, Norsk Hydro and Jeroen Goudswaard, Delft Univ.

Summary. In this paper we review the research in the DELPHI project on AVA inversion, generalized primary migration and multi-scale analysis and discuss the mutual relations.

Introduction. The relation between the angle-dependent reflectivity of an interface in a target zone and the amplitude-versus-offset (AVO) effects observed in the seismic data at the Earth's surface is complicated by many factors, as was pointed out in a classic paper by Ostrander in GEOPHYSICS in 1984. Some of these factors are 'reflection related' (such as thin bed tuning, reflector curvature), others 'propagation related' (such as geometrical spreading, transmission and/or anelastic losses) or 'acquisition related' (such as source/receiver directivity, geophone coupling). Amplitude-versus-angle (AVA) inversion in a target zone can only be carried out successfully when these effects are taken into account, either by forward modeling or by stepwise processing prior to AVA inversion. In our DELPHI research programme we opt for the latter approach.

The setup of this paper is as follows. We start by reviewing our approach to AVA inversion for migrated reflection data, assuming that all distorting effects have been optimally eliminated. Then we address the effects of transmission loss and wavelet interference related to fine-layering and discuss how to account for these effects in migration. Finally we introduce a multi-scale model for seismic reflectors and indicate how to account for this in inversion.

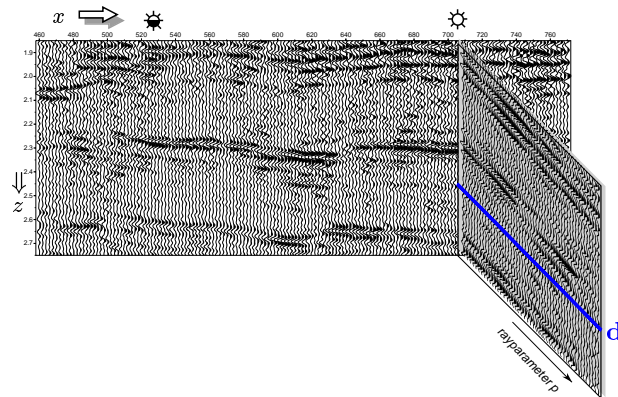


Fig. 1: Integration of a structural image and an angle-dependent reflectivity section. \mathbf{d} is the data vector used in AVA inversion.

Multi-angle inversion. Migration of multi-offset data yields, apart from a structural image, the angle-dependent reflection information for any image point in the subsurface (see e.g. Berkhout, GEOPHYSICS 1997, p 954-969). Figure 1 shows a structural image, integrated with the angle-dependent reflectivity

information along one vertical cross-section of the structural image. To be more precise, the angle-dependent reflectivity information is displayed as a function of depth z and rayparameter p , where p is related to the incidence angle θ and the local propagation velocity c , according to $p = (\sin \theta)/c$. Hence, the data vector \mathbf{d} (the blue line in Figure 1) represents the reflectivity as a function of p at one particular image point in the subsurface. In the remainder of this section we summarize the Ph.D. thesis (1998, Delft University) of the second author. We introduce the *linearized* model $\mathbf{d} = \mathbf{A}\boldsymbol{\lambda} + \mathbf{n}$, where \mathbf{A} is a matrix, derived from the Zoeppritz equation for angle-dependent PP -reflectivity, $\boldsymbol{\lambda}$ is a contrast parameter vector and \mathbf{n} is a 'noise vector' that contains all effects that are not accounted for by this linear model. For the contrast parameter vector we choose $\boldsymbol{\lambda} = (\frac{\Delta Z_p}{Z_p}, \frac{\Delta c_p}{c_p}, \frac{\Delta \mu}{\mu})^T$. Here Z_p , c_p and μ stand for P -wave impedance, P -wave velocity and shear modulus, respectively; Δ denotes the difference of the parameters below and above the interface and the bar denotes their average value. It appears that this parameterization is well-suited when only PP -data are available.

The aim of AVA inversion is to resolve the parameter vector $\boldsymbol{\lambda}$ from the data vector \mathbf{d} . To stabilize this process, a priori information can be included in the form of linear relations between the parameters, derived from rock-physics and empirical trends. This a priori information can be formulated as $\mathbf{d}_{ap} = \mathbf{A}_{ap}\boldsymbol{\lambda}_{ap} + \mathbf{n}_{ap}$. In our least-squares inversion process, the vectors \mathbf{d} and \mathbf{d}_{ap} can be given different weights, depending on the confidence that one has in the data and in the a priori information. By repeating the inversion process for all available data vectors \mathbf{d} , we obtain the estimated parameter vector $\boldsymbol{\lambda}_{est}$ for all image points of interest. The results can be displayed as depth sections in terms of the contrast parameters $\Delta Z_p/\bar{Z}_p$, $\Delta c_p/\bar{c}_p$ and $\Delta \mu/\bar{\mu}$.

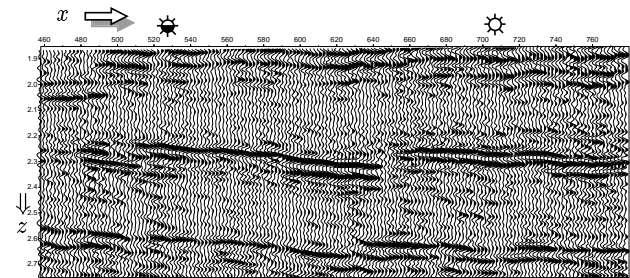


Fig. 2: Estimated P -wave velocity contrast section.

Multi-angle, multi-scale inversion of migrated seismic data: an overview

An example is given in Figure 2, which shows the $\Delta c_p/\bar{c}_p$ section, obtained from a 2D marine data set (offshore mid-Norway). The main target consists of the Jurassic sandstones in the two tilted fault blocks. The top (gas) reservoir shows up clearly as a strong reflection around $z = 2.3$ km, with a well-defined fault at $x = 650$ m. Together with the other two sections (not shown), this result can be used for further lithology discrimination.

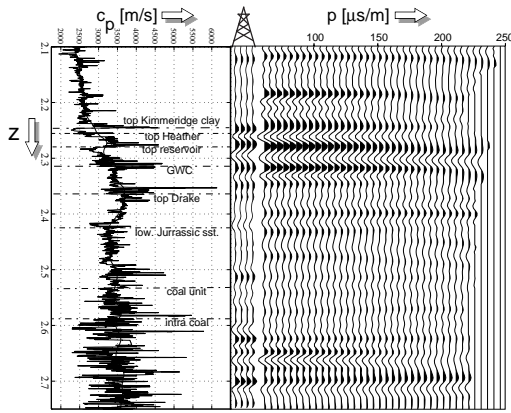


Fig. 3: Integration of well-log (P -wave velocity), synthetic impedance contrast and $\mathbf{A}\lambda_{est}$ for all image points along the well.

To validate the results, we computed $\mathbf{A}\lambda_{est}$ for all image points along one vertical cross-section. This is shown in Figure 3, together with a well-log at the same lateral position and a synthetic impedance contrast modeled from the well-log, using the adaptive scale-dependent method of Verhelst (Ph.D. thesis, 1999, Delft University). Overall there is quite a good match, but there are some notable differences as well. By analyzing the residue section $\mathbf{d} - \mathbf{A}\lambda_{est}$ (not shown) we concluded that the mismatch can be partly attributed to residual multiple reflections (only the surface related multiples were eliminated prior to migration with a 2-D algorithm).

In summary, seismic migration eliminates the propagation effects from the seismic data. Hence, the data vectors \mathbf{d} contain angle-dependent reflection information at image points in the subsurface rather than offset-dependent information at the surface. Linearized inversion of these data vectors yields the local contrast parameters for any image point in the subsurface. Obviously the quality of the inversion result depends on the accuracy of the migration algorithm (which yields the input for the inversion). Usually migration schemes account for geometrical spreading but not for transmission loss, which means that the information in the datavectors \mathbf{d} is distorted to some extent. In the next section we discuss how to compensate for this distortion.

Accounting for the effects of fine-layering. Extensive studies on wave propagation through finely layered media have shown that transmission losses and internal multiple scattering result in

an angle-dependent dispersion of the seismic wave form. Hence, ignoring these effects in migration yields dispersed images and erroneous AVA effects. Apart from these propagation related distortions, the interference of the reflection responses of reflector packages ('composite reflectors') in finely layered media causes apparent AVA effects as well. In order to account for the effects of fine-layering in migration, the following 3-D *generalized primary* representation of seismic reflection data has been developed

$$P^-(\mathbf{x}_R, \mathbf{x}_S, \omega) = \int W_g^-(\mathbf{x}_R, \mathbf{x}, \omega) \hat{R}(\mathbf{x}, \omega) W_g^+(\mathbf{x}, \mathbf{x}_S, \omega) S^+(\mathbf{x}_S, \omega) d^3\mathbf{x}. \quad (1)$$

S^+ represents the source for downgoing waves at the source point \mathbf{x}_S , W_g^+ describes generalized downward propagation into the subsurface (including transmission losses and internal multiple scattering), \hat{R} is an operator that describes reflection at any point \mathbf{x} in the subsurface, W_g^- describes generalized upward propagation to the surface and P^- represents the upgoing wave field at the receiver point \mathbf{x}_R . Note that this representation does not account for surface related multiples. In the following we shall assume that decomposition and surface related multiple elimination has been carried out.

In essence, migration based on this representation ('generalized primary migration') is accomplished by applying the inverse versions of the propagators W_g^+ and W_g^- to the data P^- , thus resolving the reflectivity operator \hat{R} . For finely layered media the inverse propagators cannot be approximated by the complex conjugate forward propagators. Correction operators are required that compensate for the transmission losses. Using reciprocity, these transmission losses, and hence the correction operators, can be estimated from the reflection measurements at the surface. The inverse propagators that are thus constructed compensate for the propagation related apparent AVA effects of fine-layering. A modified imaging step compensates for the reflection related apparent AVA effects (wavelet interference) of fine-layering. An example of an angle-dependent reflectivity section obtained by generalized primary migration of data modeled in a real well-log is shown in Figure 4a, together with the well-log of the P -wave velocity (Van Geloven et al., SEG conference, 1996). The angle-dependent amplitude information in the data vector \mathbf{d} at $z = 890$ m is shown in green in Figure 4b. It matches very well with the black curve, which represents the exact angle-dependent amplitude curve at the same depth. For comparison, the blue curve shows the angle-dependent reflectivity obtained by migration without the fine-layering corrections. Clearly generalized primary migration yields improved angle-dependent reflectivity sections. We applied the AVA inversion method discussed in the previous section to a migration result without fine-layering corrections (not shown) and to the generalized primary migration result (Figure 4a). The estimated P -wave velocity contrasts $\Delta c_p/\bar{c}_p$ are shown in Figures 5a and b

Multi-angle, multi-scale inversion of migrated seismic data: an overview

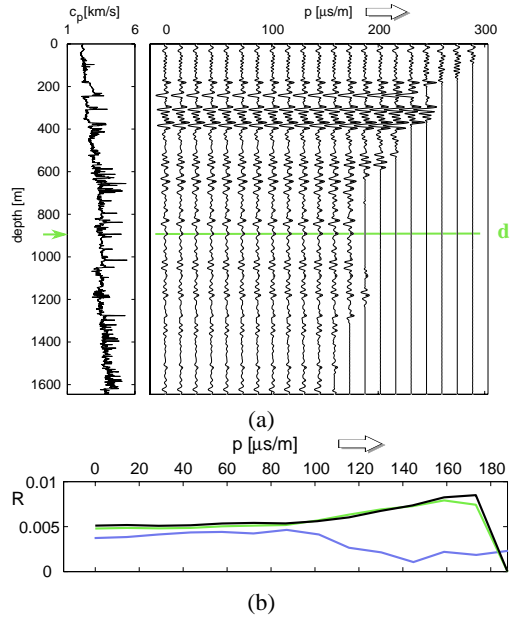


Fig. 4: (a) Integration of well-log (P -wave velocity) and angle-dependent reflectivity section, obtained by generalized primary migration. (b) Angle-dependent reflection amplitudes at $z = 890\text{m}$, obtained by migration without (blue) and with fine-layering corrections (green), obtained from figure a). The black curve is the exact result.

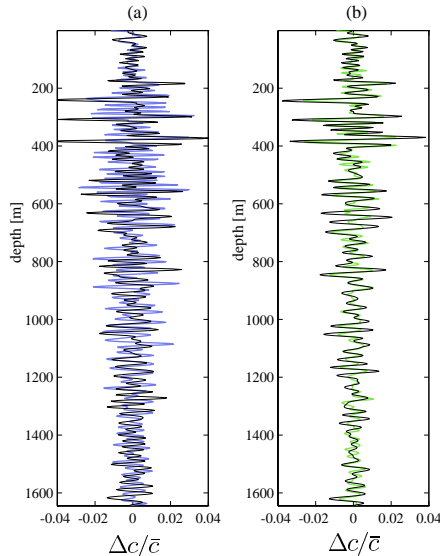


Fig. 5: AVA inversion applied to the results of migration without (a) and with fine-layering corrections (b). The blue and green curves are the inversion results, the black curves are filtered versions of the velocity log.

by the blue and green curves, respectively. The black curves in both figures are appropriately bandfiltered versions of $\Delta c_p/\bar{c}_p$,

obtained directly from the well-log. Note that the inversion result obtained after generalized primary migration (Figure 5b) matches the filtered velocity log quite accurately.

For a more detailed discussion of the effects of fine-layering and examples with multimode data, see the September/October issue of GEOPHYSICS.

In summary, generalized primary migration not only accounts for geometrical spreading but also compensates for the dispersive transmission losses and wavelet interference related to fine-layering. As a result, the apparent AVA effects are suppressed, so that the data vectors \mathbf{d} are optimally suited as input for AVA inversion. Note that for our AVA inversion we assumed so far that the data vector \mathbf{d} is related to the contrast parameter vector λ via linearized Zoeppritz equations, which implies that the medium parameters are assumed to behave as step-functions of the depth coordinate z , at least in a finite interval around the reflector. From multi-scale well-log analyses, carried out by Herrmann (Ph.D. thesis, 1997, Delft University), it appears that outliers in well-logs may behave quite differently from step-functions. In the next section we discuss how to account for 'composite reflectors' in AVA inversion.

Multi-angle, multi-scale inversion. In order to account for the complex behaviour of outliers in well-logs, we would like to generalize the parameterization of interfaces in such a way that their properties match those of real outliers and that the step-function interface can be seen as a special case. To this end we introduce the following singular function for the P -wave velocity:

$$c_p(z) = \begin{cases} c_1|z|^\alpha & \text{for } z < 0 \\ c_2|z|^\alpha & \text{for } z > 0. \end{cases} \quad (2)$$

For convenience the singular point has been chosen at $z = 0$.

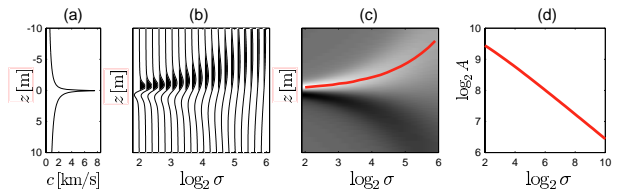


Fig. 6: Multi-scale analysis of a self-similar singularity. The slope in figure d ($\alpha = -0.4$) corresponds to the singularity exponent of the function in figure a.

For $\alpha = 0$ this function reduces to a step-function. For arbitrary α this function is self-similar, according to $c_p(\beta z) = \beta^\alpha c_p(z)$, for $\beta > 0$. For $\alpha = -0.4$, this function is shown in Figure 6a. We applied a multi-scale analysis, following the method of Mallat & Hwang (IEEE TRANS. INFORM. THEORY, 1992). Figure 6b shows the continuous wavelet transform $\tilde{c}_p(\sigma, z)$ of this function, obtained by convolving $c_p(z)$ with scaled versions of an an-

Multi-angle, multi-scale inversion of migrated seismic data: an overview

analyzing wavelet $\frac{1}{\sigma}\psi(\frac{z}{\sigma})$ (the derivative of a Gaussian). The different traces in Figure 6b correspond to different scales σ . Taking the modulus of the data in Figure 6b and connecting the local maxima from trace to trace, yields the modulus maxima line (Figure 6c). Figure 6d shows the amplitudes measured along this line, in a log-log plot. The slope of this amplitude-versus-scale (AVS) graph corresponds to the singularity exponent $\alpha = -0.4$ of the self-similar function in Figure 6a. For a step-function, the slope of the AVS curve would be zero, meaning that a step-function is scale-independent. The AVS behaviour in Figure 6d is similar to that of several outliers in real well-logs, as analyzed by Herrmann, with the restriction that for real well-logs the AVS curves reveal a 'constant-slope' behaviour only for a finite range of scales. Since seismic data are band-limited anyway, it is sufficient that our parameterization is realistic in a finite scale range. In order to resolve the multi-scale reflector properties from seismic data rather than from the well-log, a similar multi-scale analysis as discussed above should be applied to the seismic data. Dessing (Ph.D. thesis, 1997, Delft University) applied the wavelet transform to migrated seismic data for multi-scale edge detection. The application of the wavelet transform for multi-angle, multi-scale inversion is subject of the Ph.D. research of the third author. Figure 7 shows the continuous wavelet transform of the angle-dependent reflectivity section of Figure 1. The z, σ -plane (for $p = 0$) was obtained in a similar way as that in Figure 6b. The p, σ -plane is constructed of modulus maxima lines (similar to those in Figure 6c) for all available p -values; the grey-values represent the amplitudes in this modulus maxima plane. Note that this plane may be seen as a multi-scale representation of the data vector \mathbf{d} in Figure 1.

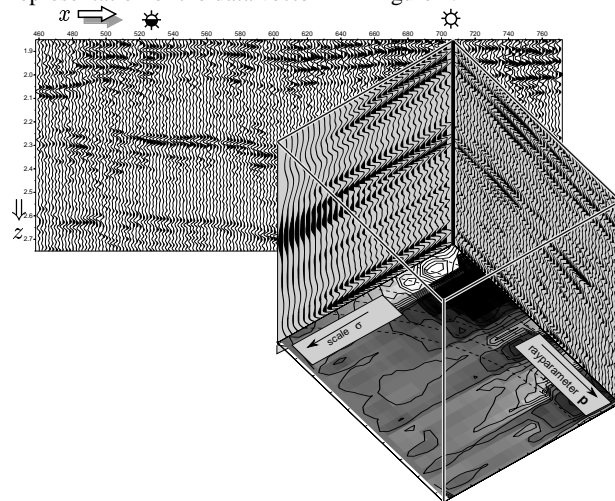


Fig. 7: Integration of a structural image, an angle-dependent reflectivity section and its multi-scale representation. The p, σ -plane is used in multi-scale AVA inversion.

The aim of multi-angle, multi-scale inversion is to resolve the parameters of a composite reflector from the p, σ -plane derived

from its reflection response. In the September/October issue of *GEOPHYSICS* we show that, for a singularity described by equation (2), the contours of constant amplitude in its p, σ -plane are described by $p^{1-\alpha}\sigma^\alpha = \text{constant}$. Hence, the singularity exponent α can be resolved by analyzing these contours. This is illustrated with an example. Figures 8a,b,c show a multi-scale analysis of a real well-log, analogous to Figure 6. The slope of the AVS curve in Figure 8c ($\alpha = -0.32$) characterizes the singularity at $z = 155\text{m}$ in the well-log of Figure 8a. Figures 8d,e,f show a multi-angle, multi-scale analysis of the migrated seismic response, analogous to Figure 7 (only the angle-dependent reflectivity section and the p, σ -plane at $z = 155\text{m}$ are shown). Using a contour matching algorithm, it appears that the contours in Figure 8f are approximately described by $p^{1-\alpha}\sigma^\alpha = \text{constant}$, with $\alpha = -0.34$. Note that this corresponds very well to the value obtained directly from the well-log.

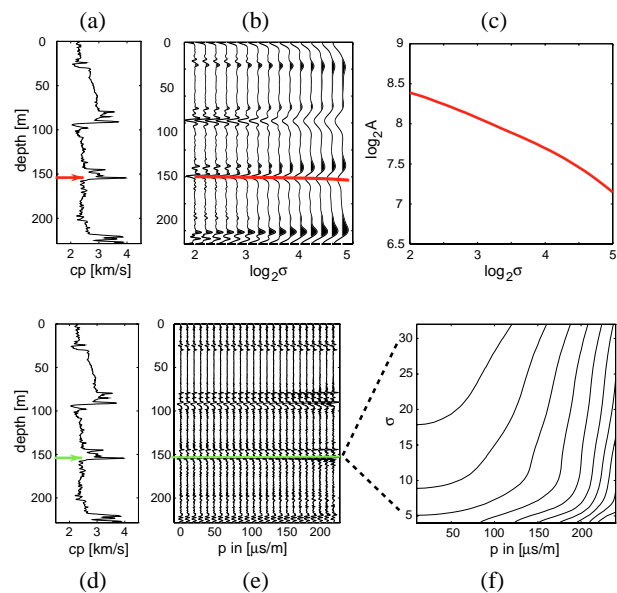


Fig. 8: (a,b,c) Multi-scale analysis of a singularity in a well-log: $\alpha = -0.32$. (d,e,f) Multi-angle, multi-scale analysis of its seismic response: $\alpha = -0.34$.

In summary, multi-angle, multi-scale inversion has the potential to resolve the parameters that characterize a composite reflector. What we have discussed is the first step towards a more general approach to multi-angle, multi-scale inversion. Ultimately we would like to resolve the elastic and petrophysical parameters of composite reflectors and relate their multi-scale parameters to the type of geological facies.

Acknowledgements. We thank the sponsors of the DELPHI consortium project and its scientific director prof A.J. Berkhout. Also the support of the Dutch Technology Foundation STW is highly appreciated.